




# Monitoring of Power Over Fiber Signals Using Intercore Crosstalk in ARoF 5G NR Transmission

Rubén Altuna , Juan D. López-Cardona , and Carmen Vázquez , *Senior Member, IEEE*

**Abstract**—Power over Fiber (PoF) needs safe and resilient operation of the infrastructure. In this article, we propose a new crosstalk-based remote monitoring technique of PoF signals in Spatial Division Multiplexing optical networks with no additional consumption at the remote radio head (RRH). We demonstrate this technique in a 250 m 7-core Multicore Fiber (MCF) transmitting three multiplexed 256 QAM 5G NR optical signals with a total throughput of 1.8 Gbps, a low-speed communications channel between a Central Office and a RRH, and a PoF signal delivering to feed the RRH's control board. The 5G NR optical signals are received at the RRH with EVM values within the limits established in the 3GPP 5G standard. The low-speed communications channel remotely manages the power supplied to a Radio Frequency Power Amplifier located at the RRH. The PoF signal is used to supply up to 131 mW to the control board of the RRH. The monitoring channel can accurately follow the optical power injected into the MCF or the optical power received at the RRH thanks to a real-time algorithm and an ad-hoc Matlab application, which also allows to control the PoF source and the low-speed communications channel.

**Index Terms**—5G new radio, centralized radio access network, intercore crosstalk, multicore optical fibers, power over fiber, spatial division multiplexing.

## I. INTRODUCTION

FIFTH-GENERATION New Radio (5G NR) wireless technology is rapidly evolving. Present and future mobile networks will feature this technology, and the number of users connected to this kind of networks is exponentially increasing. Consequently, these networks need to satisfy extremely demanding requirements in terms of latency, throughput and energy efficiency. A widely spread trend to fulfil these demands is the use of Cloud Radio Access Networks (C-RAN) architecture. This structure consists of a centralized pool of Base Band Units (BBU) placed at a Central Office (CO), where all the signal processing is performed, and a wide number of Remote Radio Heads (RRH) with reduced power consumption. The pool of

Manuscript received 15 February 2023; revised 4 July 2023; accepted 27 July 2023. Date of publication 31 July 2023; date of current version 2 December 2023. This work was supported in part by the 6G-Xtreme Project founded by UNICO-5G I+D, in part by Ministerio de Asuntos Económicos y Transformación Digital y de la Unión Europea-NextGenerationEU under Grant TSI-063000- 2021-135, in part by Spanish Research Agency under Grant PID2021-122505OB-C32, and in part by Universidad Carlos III de Madrid under Agreement CRUE-Madroño 2023. (*Corresponding author: Carmen Vázquez.*)

The authors are with the Department of Electronics Technology, Universidad Carlos III de Madrid, Leganés, 28911 Madrid, Spain (e-mail: raltuna@pa.uc3m.es; juliopez@ing.uc3m.es; cvazquez@ing.uc3m.es).

Color versions of one or more figures in this article are available at <https://doi.org/10.1109/JLT.2023.3300184>.

Digital Object Identifier 10.1109/JLT.2023.3300184

BBUs and the RRHs are connected by the fronthaul [1]. It is very convenient to use the optical domain to transmit the signal due to the small losses, reduced latency and exceptional bandwidth of optical fibers. Moreover, transmitting the signal in an analog format also helps to reduce the power consumption both in the CO and in the RRHs, since there is no need to perform analog-to-digital or digital-to-analog conversion. The transmission of Radio Frequency (RF) signals in analog format through optical fibers is known as Analog Radio over Fiber (ARoF). ARoF in C-RAN mobile networks enables high fronthaul data throughputs with good energy efficiency and scalability, and even better if Spatial Division Multiplexing (SDM) with Multicore Fibers (MCF) is used [2], [3]. In [4], a review of the most relevant achievements in SDM is presented.

The power consumption reduction in RRHs enables the use of Power over Fiber (PoF) technology to feed critical elements of the remote nodes with centralized control of the optical power supply [5]. For instance, in [6], a 14.43 km dedicated PoF link (power signal travels alone through the fiber) to feed critical parts of RRHs is presented and analyzed. In [7], an ARoF link coexisting with PoF through a Single Mode Fiber (SMF) in a shared scenario (data and power signals travel through the same core) is experimentally tested for different link lengths. More exhaustive analysis regarding interactions between ARoF and PoF is tackled in [8].

The Sixth-Generation (6G) mobile technology, which aims to achieve data rates of around 1 Tbps with ultra-low latency over 3D coverage areas, also demands high capacity networks able to connect thousands of cell sites with efficient power delivery technologies like PoF, as stated in [9]. For example, in [10], a 100-GHz photoreceiver is fed at short distances through a MCF in a dedicated scenario (data and power are sent through different cores). In [11], experiments are performed on a 20 m MCF link in both shared and dedicated scenarios. To further improve energy efficiency, the PoF pooling concept has been introduced. This concept takes advantage of the centralized powering of PoF to selectively supply only the active remote nodes [12]. In [13], tests over a 10 km 7-core MCF including a 9 m wireless link with a 25.5GHz RF carrier and a throughput of 1.4 Gbps were performed. In this experiments, 40 electrical mW were delivered to the remote node. For shorter distances, higher power levels such as 11.9 electrical W were delivered from a 1064.8 nm PoF signal co-propagating with a 64-QAM OFDM signal through a 1 km 7-core MCF [14].

The high-power signals transmitted in PoF-based powering systems can cause damage in case of optical fiber malfunction

or breaking. Thus, safe and resilient operation is needed. Monitoring techniques are already part of optical networks [15], [16]. However, specific monitoring techniques must also be introduced to observe that optical power is being correctly delivered in PoF systems. Ideally, no additional power consumption should be added to the RRHs in order to keep a good energy efficiency. Monitoring techniques in MCF links include measuring the crosstalk variation with the power meter method [17], with multichannel [18] or bidirectional [19] OTDR techniques in installed fibers. However, no monitoring techniques are reported so far specifically for PoF systems apart from [20] where a MCF in a shared scenario is monitored but considering only a single data channel, no statistical characterization neither processing of the monitoring signal with specific algorithms.

In this article, we propose a novel crosstalk (XT)-based monitoring technique for PoF signals in SDM systems. In this technique, we consider for the first time:

- the intercore XT in MCFs as a way to monitor the correct feeding of PoF signals at the remote RRH with capability to rapidly detect any link break or malfunction without interfering good quality 5G-NR data transmission neither interaction with a low speed control channel from the CO to the RRH,
- experimental demonstration of the monitoring technique on a 250 m link of 7-core MCF in a 2 W PoF shared scenario with simultaneous transmission of three wavelength-multiplexed 5G NR 256 QAM ARoF signal with a baseband bandwidth (BW) of 100 MHz carried by a 20 GHz RF carrier; providing a total throughput of 1.8 Gbps,
- the integration of a statistical processing of the XT signal received at the CO that compensates the XT fluctuations or walkoff present in MCFs to avoid errors on the measuring technique.

In this article, Section II describes the operation principle. Section III explains the experimental set-up including the three different transmitted signals: an up-to 2 W PoF signal at 1480 nm, three wavelength-multiplexed 5G NR 256QAM ARoF modulating a 20 GHz RF carrier, a low speed control channel at 1310 nm. Next, Section IV includes experimental results of noise and XT fluctuations along with measurements of the implemented technique in real time showing the good performance and no interaction with the other transmitted signals. Finally, Section V presents the conclusions.

## II. OPERATION PRINCIPLE

Optical signals propagating through MCFs suffer from intercore crosstalk (XT), which is a partial optical power coupling from the propagating core to adjacent cores. XT depends on the MCF parameters and XT after fiber propagation is a statistic value. According to [21] the mean value of the probability distribution of XT, i.e., the mean crosstalk  $XT_\mu$  happening at the MCF is given by:

$$XT_\mu = 2\sigma^2 = \frac{2\kappa \cdot R \cdot L}{\beta \cdot D_{mn}} \quad (1)$$

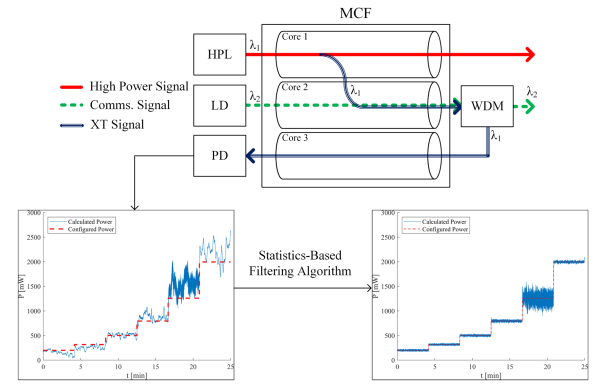


Fig. 1. Schematic of the operation principle.

$$\sigma^2 = \frac{\kappa \cdot R \cdot L}{\beta \cdot D_{mn}} \quad (2)$$

being  $\kappa$  the coupling coefficient of the MCF,  $R$  the bending radius of the MCF,  $L$  the length of the MCF,  $\beta$  the propagation constant and  $D_{mn}$  the distance between cores.

The mean crosstalk from multiple cores to one core can be represented as a sum of the mean crosstalk from each of the multiple cores to the single core, because the mean crosstalk is linearly proportional to variance, and the variance can be summed in such cases [21]. By measuring the XT in only one core, the contributions of all different cores are considered.

We propose using XT signals in a PoF system based on MCF to infer how much power from the high-power laser (HPL) is arriving to the RRH by sending it back to the CO through one of the cores of the MCF. Fig. 1 shows a simplified schematic where a high-power signal and a communication signal travel through different cores of a MCF. The XT induced by the high-power signal over the middle core is separated from the communications signal and sent back through the remaining core to be detected. Because of the stochastic evolution of XT, we need to compensate  $\sigma^2$  in order to successfully calculate the optical power travelling through the MCF; we use a statistics-based algorithm. Lower part of Fig. 1 shows influence of XT evolution on detected power for different HPL power levels without (left side) and with (right side) this filtering algorithm.

As an advantage, the core used to send back the XT signal can be used to transmit other signals. Therefore, there is no need when implementing this technique to rearrange the signals in an already existing system, only to add a Wavelength Division Multiplexer (WDM) to separate the XT from the other signals.

In high-power signal transmission, Stimulated Raman Scattering (SRS) and Stimulated Brillouin Scattering (SBS) appear after certain power levels. These thresholds  $P_{SRS}$  and  $P_{SBS}$  are [22]:

$$P_{SRS} = \frac{16 \cdot A_{eff}}{g_R \cdot L_{eff}} \quad (3)$$

$$P_{SBS} = \frac{21 \cdot k \cdot A_{eff}}{g_B \cdot L_{eff}} \cdot \frac{\Delta v_B + \Delta v_P}{\Delta v_B} \quad (4)$$

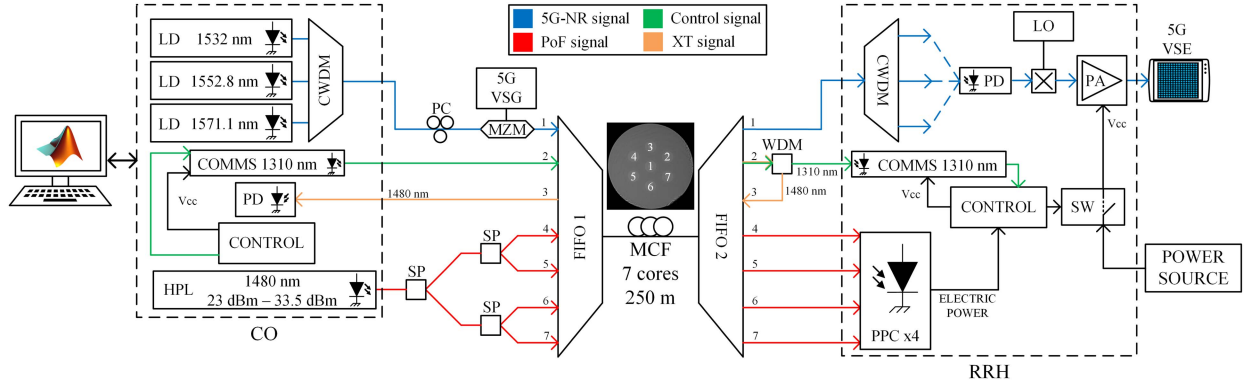


Fig. 2. Schematic of PoF monitoring technique integrated in the experimental set-up with additional functionalities. CO = Central Office, LD = Laser Diode, COMMS = Communications, PD = Photodetector, HPL = High Power Laser, PC = Polarization Controller, VSG = Vector Signal Generator, VSE = Vector Signal Explorer, MZM = Mach-Zehnder Modulator, SP = Splitter, FIFO = Fan In-Fan Out, MCF = Multicore Fiber, CWDM = Coarse Wavelength Division Demultiplexer, LO = Local Oscillator, PA = Power Amplifier, PPC = Photovoltaic Power Converter, RRH = Remote Radio Head, SW = Switch.

with  $k = 2$ ,  $A_{eff}$  effective area of the optical fiber,  $g_B$  Brillouin gain coefficient,  $\Delta_{VB}$  Brillouin gain bandwidth,  $\Delta_{VP}$  pump laser linewidth, and  $g_R$  Raman gain coefficient.

Equation (4) shows that  $P_{SBS}$  depends on the pump laser linewidth. Using a HPL with a wide linewidth, as a Raman laser, and knowing that  $g_R \ll g_B$  for all wavelengths, makes  $P_{SRS} \ll P_{SBS}$ . Previous simulations in a 7-MCF with effective areas of  $27 \mu\text{m}^2$  [23], show that SRS dominates over SBS for an 8 GHz HPL linewidth and there is no SBS impact at 5 km. Meanwhile SRS appears only for a 10 km 7-MCF when optical powers over 1.3 W are injected. Also, in [13], PoF and 5G NR transmission over a 10 km 7-MCF in a dedicated scenario injecting around 500 mW was successfully tested. The possible influence of non-linear effects on the technique needs to be addressed for each specific case, depending on link length and power levels. Anyway, as part of the calibration to implement the filtering algorithm we characterize the behavior of the XT in the system by measuring it for every HPL output power.

### III. EXPERIMENTAL SETUP

The experimental setup used in this work is shown in Fig. 2. This setup is intended to simulate a real SDM system where our monitoring technique can be demonstrated. It can be divided into three stages: the CO, the transmission medium and the RRH.

In the CO, all the signals are generated and the XT measurement is performed. To generate the PoF signal, a 1480 nm High Power Laser (HPL) able to generate up to 2 W is used. Secondly, three Laser Diodes (LD) of 1532 nm, 1552.8 nm and 1571.1 nm generate the optical carriers for the 5G NR ARoF signals. These three signals are multiplexed using a Coarse Wavelength Division Multiplexer (CWDM) and modulated using a Mach-Zehnder Modulator (MZM). To generate the 5G NR baseband signal and the electrical carrier, a R&S SMW200 A Vector Signal Generator (VSG) was used. The low-speed control signal is generated by a communications board and a control board working together. The control board receives commands from an external PC via USB and sends them to the

communications board, which converts them to the optical domain and sends them to the RRH as in [6].

The transmission medium is a 250 m long 7-core MCF with a core diameter of  $9.5 \mu\text{m}$  and a core-to-core distance of  $38.5 \mu\text{m}$ . The three multiplexed 5G NR signals are transmitted through core 1 of the MCF. The low speed control channel is injected in core 2. The PoF signal is divided by using three 1x2 optical splitters and transmitted through cores 4 to 7. Core 3 is reserved to send the XT signal back, see Fig. 2. The signals were arranged in this way because, as (2) shows,  $\sigma^2$  increases when the distance between cores decreases. Since core 1 is closest to the rest of the cores than any other in the MCF, it is less suitable to transmit the PoF signal or measure the XT. Therefore, we reserved core 1 for the 5G NR transmission, taking advantage of the fact that it is not harmed by the PoF signal, as it is shown in Section IV. Since cores 2 and 3 present lower losses than the rest, we used them to extract and send back the XT signal respectively, which are the weakest signals in the system. The remaining cores (cores 4–7) were used for the PoF transmission.

At the other end of the MCF, the three 5G NR signals are demultiplexed using a CWDM and detected using a high-speed Photodetector (PD). In the electrical domain, the 20 GHz electrical carrier is converted to 1 GHz using a mixer and a R&S SMB 100 A signal regenerator and amplified with a low-noise RF Power Amplifier (PA). The frequency conversion of the RF carrier is down converted so that the 5G NR signals can be analyzed with a R&S RTO 1022 oscilloscope, which bandwidth is 2 GHz. To evaluate the quality of the 5G NR signals, the RTO 1022 is connected to the R&S Vector Signal Explorer (VSE) software, which provides information about power spectrums, electrical power, received constellations or Error Vector Magnitude (EVM) of the received signals. This last parameter will be used to evaluate the quality of the 5G NR signals transmission. The low-speed control signal transmitted through core 2 is connected to a communications board that performs an electrical-to-optical conversion of the signal and transmits it to a control board. This control board commands an electrical switch that manages the PA's power supplying. This way, the RRH's power consumption can be remotely reduced. From core 2, the XT signal is also

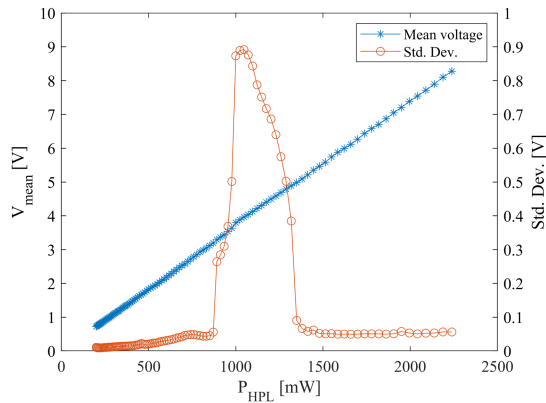


Fig. 3. Signal proportional to the HPL mean power and noise characterization.

extracted using a demultiplexer and injected back into the MCF through core 3. The PoF signal, which is transmitted through four different cores of the MCF, is connected to four commercial Photovoltaic Power Converters (PPC) connected in parallel. These PPCs can manage up to 200 mW each. The electrical power obtained from the PPCs feeds the control board that commands the electrical switch. The power consumption values of the PD, the PA and the control board, which are the main elements of the RRH, are 150 mW, 650 mW and 40 mW respectively. The power consumption of the LO and the 5G NR VSE were not taken into account because their only purpose is to measure the 5G NR signals, and in a real system they would not be present.

#### IV. EXPERIMENTAL RESULTS

We have performed a Back-to-Back (B2B) characterization of the CW fiber Raman HPL at 1480 nm from 23 dBm to 33.5 dBm in steps of 0.1 dB, measuring with a *PDA20CS2* PD and a fast oscilloscope the average power and standard deviation. We took 60000 voltage samples for each optical power. Results are shown in Fig. 3. Higher standard deviations are present in the noisy region from around 1 W to 1.4 W. As an example, at 30 dBm there is a clear sine tone of 135 kHz. This behavior can be related to the Transverse Mode Instability (TMI) effect, which appears in Raman lasers due to fast TMI mode competition power exchange or thermal diffusion dynamics within the doped fiber [24]. An energy transfer between transverse modes occurs, generating an unstable output. In [25], TMI is analyzed for two different pump wavelengths, obtaining similar results to us.

A PoF transmission characterization was also performed. Using the 1480 nm HPL, 23 dBm optical power was injected through each one of the seven cores individually, and both the transmission losses and the XT induced in the rest of the cores were measured. The transmission losses through every core at 1480 nm are between  $-2.5$  dB and  $-3$  dB, and XT values range from  $-40$  dB to  $-60$  dB. The maximum optical power received at the RRH was also measured, up to 100 mW per core. We measured the maximum electrical power that the PPCs generate by obtaining the IV and PV curves for that incident optical power. Fig. 4 shows the results for the four PPCs connected in parallel. The maximum electrical power extracted from the

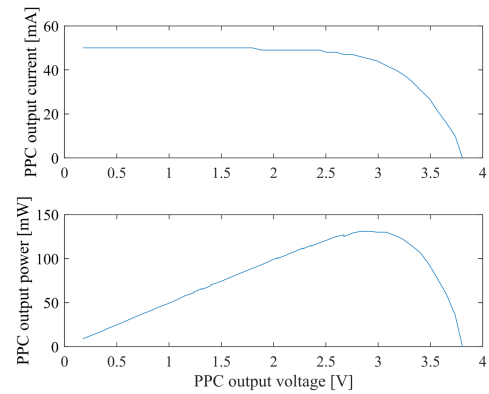


Fig. 4. IV and PV curves for four PPCs connected in parallel and receiving 100 mW each.

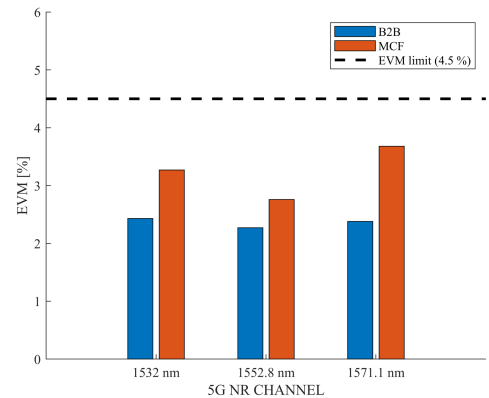


Fig. 5. Minimum EVM of the three 5G NR channels. Blue bars represent the EVM in B2B scenario. Red bars represent EVM with MCF link.

four PPCs is 131 mW, which is enough to feed three different RRH controllers.

Next, we evaluated the 5G NR signal transmission quality. We first tested the quality of the 5G NR signal received at the RRH in a B2B scenario, that is, removing the MCF from the setup. The maximum EVMs are 2.43% for the 1532 nm channel, 2.27% for the 1552.8 nm channel and 2.38% for the 1571.1 nm. Once the B2B scenario was tested, we added the MCF to the setup. We observed that the maximum EVM increased to 3.27% for the 1532 nm channel, 2.76% for the 1552.8 nm channel and 3.68% for the 1571.1 nm channel. Even though all three channels worsen when the MCF is included, they all are under the 4.5% limit established by the 5G NR standard. The difference in the EVM increase between the different channels is caused by the MCF's FIFOs, which are designed for 1550 nm and have bigger losses at 1532 nm and 1571.1 nm. Fig. 5 presents a summary of the results. We also checked if the PoF signal affected the 5G NR signals when simultaneously transmitted, and no influence was observed. In [13], this same measurement was performed for a 10 km 7-core MCF delivering up-to 133 mW, and no impact from the PoF signal to the 5G NR signal was observed. In [11], BER measurements were performed in shared and dedicated



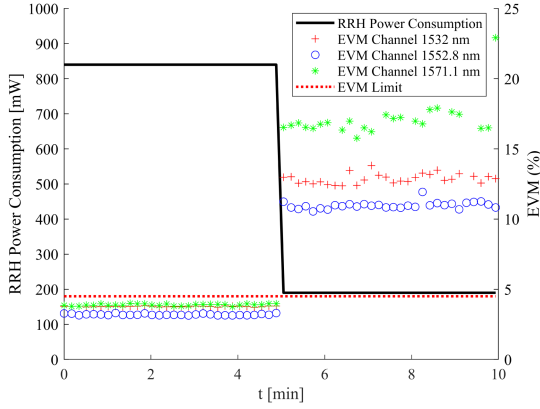


Fig. 6. RRH power consumption and EVM evolution over time.

scenarios on a 4-core MCF launching 200 mW. No influence in the dedicated scenario was observed.

We checked the low-speed control channel by using a command to toggle the electrical switch located at the RRH. We measured the electrical power consumed by the PD, the PA and the control board of the RRH as well as the EVM of the three 5G NR communication channels every 10 seconds over 5 minutes, and then we sent the command to toggle the electrical switch and repeated the measurement. The results are shown in Fig. 6. For the first 5 minutes, when the electrical switch is on, the EVM of the three 5G NR channels range from 3% to 4%, and the RRH total power consumption remains constant at 840 mW. When the command to turn off the electrical switch is sent, the RRH total power consumption is reduced to 190 mW, which is a 77.4% reduction. As a consequence of turning off the PA, the EVMs of the 5G NR channels increase by 10–12%. This test demonstrates the capability to remotely control the RRH from the CO and that the power consumption of the RRH can be significantly reduced. Similarly to the case of the 5G NR channels, we do not expect any interaction between the PoF signal and the control channel.

Once the PoF, the 5G NR and the low speed communication channels were checked, we assessed the PoF monitoring technique. We first tested the behavior of the XT signal detected back at port 3 of the MCF (see Fig. 2) when PoF signals are injected through cores 4 to 7. We configured the HPL to inject two different optical powers and took 1800000 samples in each case. Results are shown in Fig. 7. The upper graph shows a 30-minute measurement of two XT signals for optical input powers of 25 dBm and 30 dBm. In both cases, a slow variation can be clearly seen. This variation is caused by the stochastic evolution of the XT in MCF, which is described in [21] as a chi-square distribution with the following probability density function (PDF):

$$f^{\sigma^2}(XT) = \frac{1}{2\sigma^2} \exp\left(-\frac{XT}{2\sigma^2}\right) \quad (5)$$

The lower graph in Fig. 7 shows the PDF for both measured XT signals of upper graph. The XT for a 25 dBm HPL looks like a chi-square distribution. In the case of 30 dBm, a higher frequency noise can also be seen, generating a wider distribution

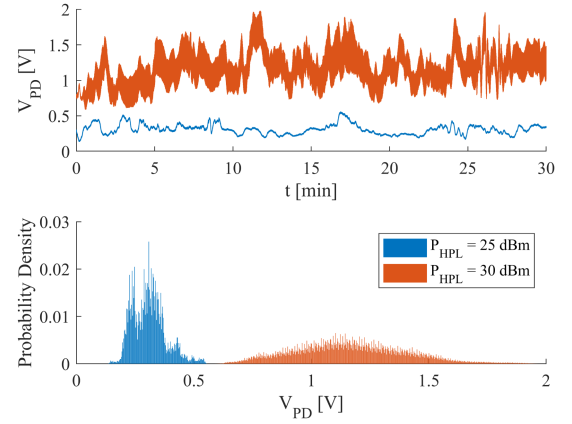


Fig. 7. Upper graph: detected XT signal for HPL optical power of 25 dBm (blue) and 30 dBm (orange). Lower graph: Probability distributions of the signals shown in the upper graph.

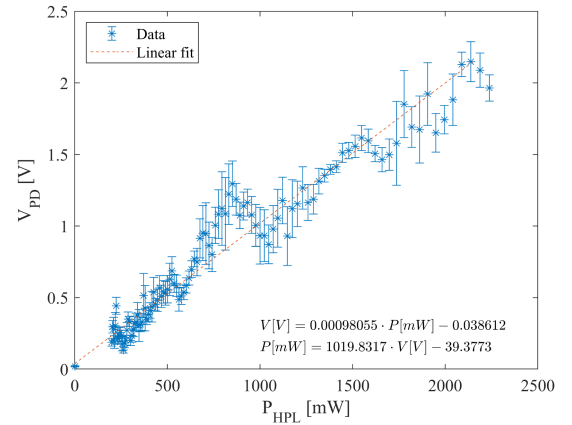


Fig. 8. Signal proportional to the XT detected at CO versus the HPL optical power.

(see lower graph). This noise mostly comes from the HPL, as shown in the previous characterization, additionally to the fact that the measured data for HPL powers of 33 dBm adjust again to a chi-square distribution.

The slow oscillations caused by the XT are complicated to filter out, requiring a specific signal processing. Having each measured XT signal a specific PDF we can differentiate between expected voltage values and anomalous voltage values for each HPL optical power if the mean voltage  $V_\mu$  and the standard deviation  $\sigma_V^2$  in each case are known. Therefore, we measured this couple of values for all the HPL power range. Fig. 8 presents the mean voltage  $V_\mu$  and the standard deviation  $\sigma_V^2$  detected by the *PDA20CS2* PD at the CO as a function of the HPL power injected into the MCF for each one of them.

Fig. 8 also shows a linear fit of the mean voltage values with a R-square goodness coefficient of 94.5% to the following equations:

$$V[V] = 0.00098055 \cdot P[mW] - 0.038612 \quad (6)$$

$$P[mW] = 1019.8317 \cdot V[V] - 39.3773 \quad (7)$$

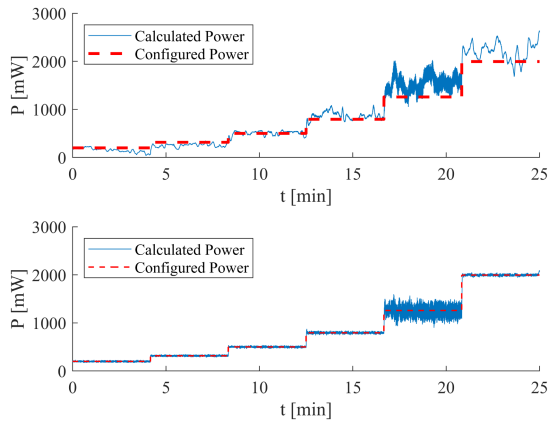


Fig. 9. HPL optical power configured and calculated without XT walkoff compensation (upper graph) and with XT walkoff compensation (lower graph).

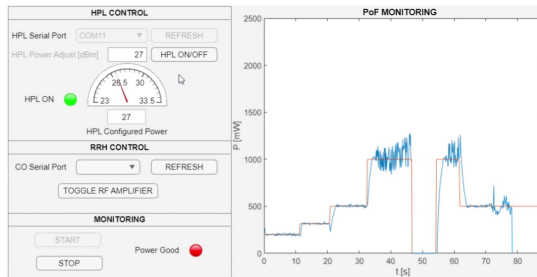


Fig. 10. Matlab ad-hoc application to control the HPL, send commands to the RRH and monitor the PoF signal in real time.

Using (7), the optical power injected by the HPL into the MCF can be inferred, and using the standard deviation represented as error bars in Fig. 8, voltage anomalies can be detected and the XT walkoff can be compensated. To do so, we developed a real-time algorithm that, knowing the optical power configured in the HPL, measures the XT signal received at the CO through core 3, checks if the voltage is within the expected values and, if so, gradually compensates the XT walkoff. The voltage limits were set to  $\bar{V} \pm 2\sigma$ , including 95.4% of the possible voltage values. All the voltage values out of the 95.4% most probable ones were considered as anomalies. This algorithm leads to real-time results as the one presented in Fig. 9. The upper graph shows the HPL optical power calculated from the voltage values in real time using (7) when the XT walkoff compensation algorithm is not being applied, and the lower graph shows the same measurement after compensation. The optical power calculated is stable thanks to the algorithm, and the noise of the HPL is perfectly detected at around 1 W. This shows that the algorithm works and compensates the XT walkoff without losing important information about the monitored PoF signal.

Lastly, all the functionalities tested were integrated into an ad-hoc Matlab application. The PC running this application was connected to the control board of the CO to send commands to the RRH, to the HPL to configure the HPL optical power, and to the PD to record the XT measurements. The application appearance is shown in Fig. 10. The controls for the HPL, the

RRH and the monitoring channel are located on the left side of the application. The HPL control is used to turn on and off the HPL and to change its optical power. The RRH control is used to send the toggle command to activate or deactivate the electrical switch at the RRH. The monitoring control turns on and off the monitoring channel and shows whether the optical power calculated from the monitoring channel matches the optical power configured at the HPL. The graph on the right side of the application shows the power configured at the HPL (orange line) and the calculated optical power in real time (blue line). The orange and the blue lines match for the whole measurement time except for the final part. At 70 seconds the MCF was disconnected, and the movement of the connectors can be seen in the oscillation of the measurement between 70 and almost 80 seconds. From 80 seconds to the end of the measurement, the monitoring channel detects a malfunction in the PoF transmission and shows it in two ways: in the graph on the right side of the application and by lighting the “Power Good” indicator red.

## V. CONCLUSION

In this work, we proposed a XT-based monitoring technique for PoF signals in SDM systems with no additional power consumption at the remote side. We tested this technique in a functional SDM link based on a 250 m 7-core MCF transmitting three multiplexed 256 QAM 5G NR signal reaching 1.8 Gbps total throughput, a low-speed communication channel to control a RRH, and a PoF signal shared between four of the seven cores of the MCF. Transmission of all signals was achieved with low transmission losses and with no negative interactions between them. The 5G NR signals were received with maximum EVMs below 4%, which meet the requirements of the 3GPP 5G standard. The low-speed communication channel controls an electrical switch located at the RRH that manages the power supply for a RF PA, allowing to decrease the RRH power consumption when necessary. The PoF signal was used to supply up to 131 mW to the control board of the RRH. Good scalability can be achieved since there was enough electrical power to supply three different RRH control boards. Thanks to a real time algorithm and an ad-hoc application developed in Matlab, the PoF monitoring channel properly follows the optical power that is injected into the MCF and allows to detect malfunctions in the PoF link, demonstrating that this technique can be used in real SDM links sharing transmission medium with different type of optical signals.

## ACKNOWLEDGMENT

The authors want to thank Fahad Mohammed Abdulhusse Al-Zubaidi for his support with VPI Photonics simulations.

## REFERENCES

- [1] C. Ranaweera, J. Kua, I. Dias, E. Wong, C. Lim, and A. Nirmalathas, “4G to 6G: Disruptions and drivers for optical access [invited],” *J. Opt. Commun. Netw.*, vol. 14, no. 2, pp. A143–A153, Feb. 2022, doi: [10.1364/JOCN.440798](https://doi.org/10.1364/JOCN.440798).
- [2] J. M. Galve, I. Gasulla, S. Sales, and J. Capmany, “Reconfigurable radio access networks using multicore fibers,” *IEEE J. Quantum Electron.*, vol. 52, no. 1, Jan. 2016, Art. no. 0600507, doi: [10.1109/JQE.2015.2497244](https://doi.org/10.1109/JQE.2015.2497244).

- [3] S. Rommel et al., "Towards a scaleable 5G fronthaul: Analog radio-over-fiber and space division multiplexing," *J. Lightw. Technol.*, vol. 38, no. 19, pp. 5412–5422, Oct. 2020, doi: [10.1109/JLT.2020.3004416](https://doi.org/10.1109/JLT.2020.3004416).
- [4] B. J. Puttnam, G. Rademacher, and R. S. Luís, "Space-division multiplexing for optical fiber communications," *Optica*, vol. 8, no. 9, pp. 1186–1203, 2021, doi: [10.1364/OPTICA.427631](https://doi.org/10.1364/OPTICA.427631).
- [5] D. S. Montero, J. D. López-Cardona, F. M. A. Al-Zubaidi, I. Pérez, P. C. Lallana, and C. Vázquez, "The role of power-over-fiber in C-RAN fronthauling towards 5G," in *Proc. 22nd Int. Conf. Transparent Opt. Netw.*, 2020, pp. 1–4, doi: [10.1109/ICTON51198.2020.9203531](https://doi.org/10.1109/ICTON51198.2020.9203531).
- [6] J. D. López-Cardona, R. Altuna, D. S. Montero, and C. Vázquez, "Power over fiber in C-RAN with low power sleep mode remote nodes using SMF," *J. Lightw. Technol.*, vol. 39, no. 15, pp. 4951–4957, Aug. 2021, doi: [10.1109/JLT.2021.3080631](https://doi.org/10.1109/JLT.2021.3080631).
- [7] F. M. A. Al-Zubaidi, J. D. López-Cardona, D. S. Montero, and C. Vázquez, "Optically powered radio-over-fiber systems in support of 5G cellular networks and IoT," *J. Lightw. Technol.*, vol. 39, no. 13, pp. 4262–4269, Jul. 2021, doi: [10.1109/JLT.2021.3074193](https://doi.org/10.1109/JLT.2021.3074193).
- [8] R. Altuna, J. D. López-Cardona, F. M. A. Al-Zubaidi, D. S. Montero, and C. Vázquez, "Power-over-fiber impact and chromatic-induced power fading on 5G NR signals in analog RoF," *J. Lightw. Technol.*, vol. 40, no. 20, pp. 6976–6983, Oct. 2022, doi: [10.1109/JLT.2022.3205743](https://doi.org/10.1109/JLT.2022.3205743).
- [9] N. Chen and M. Okada, "Toward 6G Internet of Things and the convergence with RoF system," *IEEE Internet Things J.*, vol. 8, no. 11, pp. 8719–8733, Jun. 2021, doi: [10.1109/JIOT.2020.3047613](https://doi.org/10.1109/JIOT.2020.3047613).
- [10] T. Umezawa et al., "Multi-core based 94-GHz radio and power over fiber transmission using 100-GHz analog photoreceiver," in *Proc. Eur. Conf. Opt. Commun.*, 2016, pp. 1–3.
- [11] C. Vázquez, D. S. Montero, F. M. A. Al-Zubaidi, and J. D. López-Cardona, "Experiments on shared- and dedicated- power over fiber scenarios in multi-core fibers," in *Proc. Eur. Conf. Netw. Commun.*, 2019, pp. 412–415, doi: [10.1109/EuCNC.2019.8802042](https://doi.org/10.1109/EuCNC.2019.8802042).
- [12] G. Otero et al., "SDN-based multi-core power-over-fiber (PoF) system for 5G fronthaul: Towards PoF pooling," in *Proc. Eur. Conf. Opt. Commun.*, 2018, pp. 1–3, doi: [10.1109/ECOC.2018.8535543](https://doi.org/10.1109/ECOC.2018.8535543).
- [13] J. D. López-Cardona et al., "Power-over-fiber in a 10 km long multicore fiber link within a 5G fronthaul scenario," *Opt. Lett.*, vol. 46, no. 21, pp. 5348–5351, 2021, doi: [10.1364/OL.439105](https://doi.org/10.1364/OL.439105).
- [14] H. Yang, S. Wang, D. Peng, Y. Qin, and S. Fu, "Optically powered 5G WDM fronthaul network with weakly-coupled multicore fiber," *Opt. Exp.*, vol. 30, no. 11, pp. 19795–19804, 2022, doi: [10.1364/OE.457347](https://doi.org/10.1364/OE.457347).
- [15] J. Montalvo, A. Tapetado, D. S. Montero, and C. Vázquez, "WDM-PON preventive optical monitoring system with colourless reflectors," in *Proc. Opt. Fiber Commun. Conf. Exhib.*, 2016, pp. 1–3.
- [16] P. J. Urban, G. C. Amaral, G. Żegliński, E. Weinert-Raczka, and J. P. V. d. Weid, "A tutorial on fiber monitoring for applications in analogue mobile fronthaul," *IEEE Commun. Surv. Tut.*, vol. 20, no. 4, pp. 2742–2757, Fourthquarter, 2018, doi: [10.1109/COMST.2018.2846747](https://doi.org/10.1109/COMST.2018.2846747).
- [17] T. Hayashi, T. Taru, O. Shimakawa, T. Sasaki, and E. Sasaoka, "Characterization of crosstalk in ultra-low-crosstalk multi-core fiber," *J. Lightw. Technol.*, vol. 30, no. 4, pp. 583–589, Feb. 2012, doi: [10.1109/JLT.2011.2177810](https://doi.org/10.1109/JLT.2011.2177810).
- [18] M. Yoshida et al., "Measurement of mode-coupling along a multi-core submarine fiber cable with a multi-channel OTDR," in *Proc. Eur. Conf. Opt. Commun.*, 2022, pp. 1–4.
- [19] M. Nakagawa, M. Ohzeki, K. Takenaga, and K. Ichii, "Novel inter-core crosstalk measurement method using loopback and bidirectional OTDR technique," in *Proc. Eur. Conf. Opt. Commun.*, 2022, pp. 1–4.
- [20] R. Altuna, J. D. López-Cardona, and C. Vázquez, "Crosstalk-based remote monitoring technique for power over fiber signals in spatial division multiplexing links," in *Proc. IEEE Int. Topical Meeting Microw. Photon.*, 2022, pp. 1–4, doi: [10.1109/MWP54208.2022.9997712](https://doi.org/10.1109/MWP54208.2022.9997712).
- [21] T. Hayashi, T. Taru, O. Shimakawa, T. Sasaki, and E. Sasaoka, "Design and fabrication of ultra-low crosstalk and low-loss multi-core fiber," *Opt. Exp.*, vol. 19, no. 17, pp. 16576–16592, 2011, doi: [10.1364/OE.19.016576](https://doi.org/10.1364/OE.19.016576).
- [22] J. Toulouse, "Optical nonlinearities in fibers: Review, recent examples, and systems applications," *J. Lightw. Technol.*, vol. 23, no. 11, pp. 3625–3641, Nov. 2005, doi: [10.1109/JLT.2005.855877](https://doi.org/10.1109/JLT.2005.855877).
- [23] C. Vázquez et al., "Multicore fiber scenarios supporting power over fiber in radio over fiber systems," *IEEE Access*, vol. 7, pp. 158409–158418, 2019, doi: [10.1109/ACCESS.2019.2950599](https://doi.org/10.1109/ACCESS.2019.2950599).
- [24] V. Distler et al., "Experimental analysis of Raman-induced transverse mode instability in a core-pumped Raman fiber amplifier," *Opt. Exp.*, vol. 29, no. 11, pp. 16175–16181, 2021, doi: [10.1364/OE.424842](https://doi.org/10.1364/OE.424842).
- [25] B. Yang et al., "High power monolithic tapered ytterbium-doped fiber laser oscillator," *Opt. Exp.*, vol. 27, no. 5, pp. 7585–7592, 2019, doi: [10.1364/OE.27.007585](https://doi.org/10.1364/OE.27.007585).

**Rubén Altuna** received the M.Sc. degree in electronics systems engineering in 2020 from the Universidad Carlos III of Madrid, Getafe, Spain, where he is currently working toward the Ph.D. degree in electrical, electronics and automation engineering. His research interests include radio over fiber, multicore optical fibers, instrumentation and power over fiber systems.

**Juan D. López-Cardona** received the M.Sc. degree in electronics systems engineering from the Charles III University of Madrid, Spain, in 2016, and the Ph.D. degree in electrical, electronics, and automation engineering in 2022. His research interests include low power electronics, biomedical applications, multicore optical fibers, low power electronics, and power over fiber systems.

**Carmen Vázquez** (Senior Member, IEEE) received the Ph.D. degree in photonics from the Telecommunications Engineering School, Polytechnic University of Madrid, Madrid, Spain, in 1995. She received the Fellowship with TELECOM, Denmark, in 1991, working on erbium-doped fiber amplifiers. From 1992 to 1995, she was with Optoelectronics Division, Telefónica Investigación y Desarrollo. She was involved in III-V integrated optics devices characterization, design, and fabrication. In 1995, she joined Charles III University of Madrid, Getafe, Spain, where she is currently a Full Professor and the Head of the Displays and Photonic Applications Group. She was a Visiting Scientist with the Research Laboratory of Electronics, Massachusetts Institute of Technology, Cambridge, MA, USA, from 2012 to 2013, working on silicon photonics. Her research interests include integrated optics, optical communications and instrumentation, including, plastic and multicore optical fibers, broadband access networks and monitoring techniques, RoF systems, power over Fiber, fiber optic sensors, and 5G & WDM networks. She was leading Principal Investigator on PoF at BlueSPACE (Building on the Use of Spatial Multiplexing 5G Networks Infrastructures and Showcasing Advanced technologies and Networking Capabilities) and now coordinates 6G-Xtreme project. She is a Fellow of SPIE.